

# A biophysical model for simulation and rational design of self-organized structures in artificial tissue

J.P. Hague,<sup>1</sup> P.W. Mieczkowski,<sup>2,1</sup> C. O'Rourke,<sup>3</sup> A.J. Loughlin,<sup>2</sup> and J.B. Phillips<sup>4,3</sup>

<sup>1</sup>*School of Physical Sciences, The Open University, Milton Keynes, MK7 6AA, UK\**

<sup>2</sup>*School of Life Health and Chemical Sciences, The Open University, Milton Keynes, MK7 6AA, UK*

<sup>3</sup>*UCL Centre for Nerve Engineering, London, UK*

<sup>4</sup>*Department of Pharmacology, UCL School of Pharmacy, London, WC1N 1AX, UK*

We develop a biophysical model for predicting self-organization and reshaping of artificial tissue due to the microscopic active forces between cells and the extracellular matrix (ECM), which we solve using simulated annealing, obtaining close agreement with experiment. The feedback between active forces generated by cells, and the extracellular matrix within which they exist, is a process central to the macroscopic self-organization and reshaping of tissues. There is a need to: (1) construct biophysical models, that can simulate these processes for the very large number of cells found in artificial tissues, (2) validate and calibrate those models against experimental data, (3) understand the active feedback between cells and the extracellular matrix, and its relationship to macroscopic self-organization and reshaping of tissues, to develop better design techniques for artificial biological tissues. The biophysical model that we develop to understand this active feedback consists of a contractile network representing the ECM, that interacts with a sufficiently large number of cells to describe macroscopic self-organization and reshaping of tissue. We solve the model using simulated annealing, validating our simulations against artificial neural tissue grown in a range of molds, and show how model parameters can be calibrated using untethered tissue grown in multiwell plates. We conclude that symmetry is a key factor in the active forces that drive complex, yet predictable, macroscopic self-organization and reshaping of tissue. We discuss important applications of the biophysical model to simulation and rational design of artificial tissues that could be used in pharmaceutical testing and regenerative medicine.

## I. INTRODUCTION

There is a need for new biophysical simulation capabilities that can understand and predict the onset of self-organization in artificial tissues. For example, it is critical that cells in artificial nervous and corneal tissues are self-organized so that they are highly aligned [1–4]. This alignment is similar to the nematic order found in liquid crystals, raising the possibility that minimal models of the type used in statistical physics could be used to simulate artificial tissues. In this paper, we introduce and discuss such a biophysical model.

A key factor in the self-organization and reshaping of tissues is active feedback between microscopic forces generated by cells and macroscopic tensions in the extracellular matrix (ECM). Cells in tissues grow within ECM, a biopolymer network with viscoelastic properties. Cells generate active forces that locally distort the ECM, and also respond to tensions in the ECM. If sufficient numbers of cells act in the same way, the resulting macroscopic tension reshapes the tissue, and also directs self-organization in the tissue in a feedback loop. Examples of how cells in hydrogels influence the shape of the tissue can be seen in Fig. 1, which shows cell-induced contractions in both untethered artificial tissues, and the use of tethers to guide tension in the engineered tissue. Due to the tension fields from these microscopic distortions and macroscopic reshaping of the ECM, regions of both

self-organization and disorder are found within the engineered tissue samples [5].

The goal of this paper is to obtain greater insight into the processes of ECM-cell interaction, by using numerically solved biophysical models, and to assess the potential for application of these techniques to the rational design of the scaffolds and molds used for growing artificial tissue. Tissues are active materials that manifest self-organized order and spontaneous symmetry breaking due to the local reactions of cells to the global properties of their environment and vice versa. We aim to develop a biophysical model that (1) is sufficiently complex to incorporate the physics of the subtle interplay between the extracellular matrix and active forces in cells; (2) can simulate the reshaping process and self-organization on a macroscopic scale; (3) is sufficiently simple to describe large numbers of cells in tissue structures. Hence, we aim to generate techniques for detailed large-scale simulations of self-organization in artificial tissues that can be used as tools to assist rational design of molds and scaffolds.

Theoretical models have been used successfully to describe the shapes of both tethered single cells [6] and bulk tissue [7–9], but such models do not include the macroscopic reshaping and self-organization of tissue that originates from the feedback between active forces in cells and local tensions in the ECM. To simulate this process, one could look to previous biophysical models of cell orientation. For example, a force-dipole approach could be used to simulate the interactions between cells and the ECM (see e.g. [10]). Since it has been established that

---

\* Correspondence: Jim.Hague@open.ac.uk

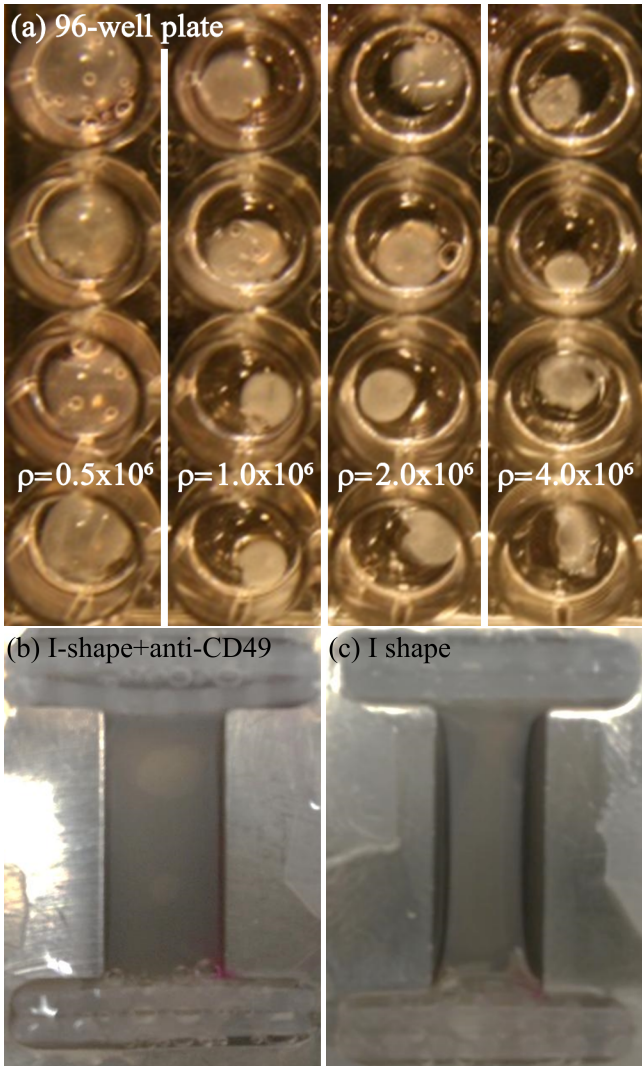


FIG. 1. Examples of artificial neural tissues, seeded with glial cells: (a) free-floating tissues in 96-well plates, showing contraction on increasing density (left to right); (b) and (c) tissues in an I-shaped mold, where reshaping of the ECM is modified by tethers. In panel (b), anti-CD49 antibodies are used to block integrins. The cells in panel (c) are self-organized at the center of the sample (not shown). Reproduced from Ref. [5]

cells find an orientation consistent with the minimum work needed to obtain that configuration [11], it would then suffice to find the lowest energy (ground) state of the theoretical model. However, the cells in such force-dipole models must be constrained to occupy nearly-fixed positions in their substrates to avoid volume collapse relating to the form of the interaction (which has a  $1/r^3$  attractive form). Thus, such models cannot describe the reshaping of tissue that occurs concurrently with self-organization. Alternatively, one could use contractile network models [6] to study the ECM under tension, since tissues can distort according to the stresses upon them. However, such an approach does not include the active forces of

cells. Thus, neither approach on its own contains sufficient biophysics to describe the feedback between macroscopic and microscopic processes, and new approaches are needed.

Our microscopic computational biophysical model of self-organization in artificial tissue, combines a complex network of elastic fibers with fundamental symmetry considerations relating to glial cells, to describe the active feedback between cells and ECM, that leads to the macroscopic self-organization and reshaping of tissues found in experiments. We know from experiments that even in the absence of initial tension, cells in tethered artificial tissues play an active role to remodel the ECM. As we shall show, this active role of cells is an essential part of the self-organization process. Our approach to simulating this effect is different to previous work, with emphasis on a mixed phenomenological and biophysical model that is fast to run, yet sufficiently detailed to make predictions for extremely large numbers of cells.

Our CONtractile Network Dipole ORientation (CONDOR) model of cellular self-organization goes beyond previous work by combining force-dipole models with contractile network models. It is able to describe the tension fields, self-organization, and reshaping of tissues that arises from the active forces between cells and ECM. Spring networks are a popular way of representing elasticity in biopolymers [12], and force-dipoles are a successful way of representing ordering of cells in tissues [10], but have not yet been combined in this way.

Beyond the description of tissues, the CONDOR model could assist in the rational design of the scaffolds and molds, that direct self-organization in engineered (or artificial) tissues. Artificial tissues are important in both pharmaceutical testing and regenerative medicine. In order to be useful for these applications, engineered tissues need to mimic the properties of real tissues. The development of new molds and scaffolds to encourage biologically relevant self-organization can take many months or years of painstaking trial and error. So developing computational tools to predict which mold designs have a good chance of success is of significant interest.

This paper is organised as follows. In Sec. II, the CONDOR model and simulated annealing method for solving it are introduced. We present detailed comparisons between simulation results and experimental data in Sec. III. Finally, in Sec. IV we conclude and discuss how our simulation could be used for rational design of artificial tissue molds.

## II. METHOD AND CONDOR MODEL

In this section, we develop the CONDOR biophysical model that we use to describe how the active feedback between cells and ECM leads to reshaping of, and self-organization in, tissues; discuss how the parameters of the CONDOR model can be related to the cell density; and describe details of the simulated annealing method

that we use to solve the CONDOR model.

### A. Development of the CONDOR model for self-organization in engineered tissue

The biophysical model developed here is based on a network of springs representing the ECM, with the interactions between cells and ECM dictated by the symmetry of the cells. The cells in the artificial tissue structures that we simulate here are well separated, such that there is no direct interaction between cells; rather, the interaction is mediated via the ECM. The glial cells considered here (and many other cell types) are naturally elongated, and thus assumed to have approximately order 2 rotational symmetry. This order 2 correction is consistent with a force dipole.

In the absence of cells, the energy of the spring network representing the ECM is given by a sum over Hooke's law for each individual filament,  $E = \frac{1}{2} \sum_{ij} \kappa_{ij} (|\mathbf{l}_{ij}| - l_{\text{eq},ij})^2$ . Here,  $\mathbf{l}_{ij}$  is the displacement between cells at vertices  $i$  and  $j$ ,  $l_{\text{eq},ij}$  is the equilibrium length between springs and  $\kappa_{ij}$  is the spring constant.

We introduce the effect of the active forces generated between cells and the network, via a modification of the

equilibrium length of the neighboring springs,  $l_{\text{eq},ij} = l_0 - f(\Theta_{1,ij}, \Theta_{2,ij})$ .  $l_{0,ij}$  is the equilibrium length of the bond in the absence of cells,  $\Theta_{1,ij}$  and  $\Theta_{2,ij}$  are the angles between a bond and cell orientations at the end of the bond. For simplicity, cells are positioned at the vertices between springs. Cells are able to remodel, pull on and respond to the extracellular matrix [13], and as such the tissue sample, which is a material comprising both ECM and cells, is active and can generate its own stresses. It is noted that the modification we consider here represents the end result of the active processes, rather than the time-dependent details of such processes.

A form of  $f$  consistent with order 2 symmetry is,

$$f(\Theta_{1,ij}, \Theta_{2,ij}) = l_{0,ij} \frac{\Delta_{ij}}{2} (2 - \cos^2(\Theta_{1,ij}) - \cos^2(\Theta_{2,ij})), \quad (1)$$

where  $\Delta < 1$  is a dimensionless constant controlling contraction perpendicular to the long axis of the cell. For each bond,  $\cos(\Theta_{ij}) = \hat{\mathbf{l}}_{ij} \cdot \hat{\mathbf{s}}_i$ , where  $\hat{\mathbf{s}}_i$  is a unitary vector representing the orientation of the cell and  $\hat{\mathbf{l}} = \mathbf{l}_{ij}/|\mathbf{l}_{ij}|$ . There are two length corrections, since there are cells at both ends of the bond (spring).

Thus, taking into account the effects of corrections to the length, the total energy of the CONDOR model is,

$$E = \sum_{ij} \frac{\kappa_{ij}}{2} \left( |\mathbf{l}_{ij}| - l_{0,ij} \left( 1 - \frac{\Delta_{ij}}{2} (2 - |\hat{\mathbf{l}}_{ij} \cdot \hat{\mathbf{s}}_i|^2 - |\hat{\mathbf{l}}_{ij} \cdot \hat{\mathbf{s}}_j|^2) \right) \right)^2 \quad (2)$$

A schematic of the CONDOR model can be seen in Fig. 2.

The spring network used here is constructed on a regular lattice, and it is important to select a lattice with appropriate shear moduli to represent the ECM. Spring networks constructed from square or simple cubic lattices have zero shear modulus [12]. Thus our fully three dimensional simulations are carried out using face-centered-cubic (FCC) lattices of cells, since the tetrahedral structures in these lattices ensure shear modulus. The shear and bulk moduli of the ECM, can be controlled more subtly through the ratio of next-nearest neighbor (NNN) to near neighbor (NN) coupling,  $\kappa_{\text{NNN}}/\kappa_{\text{NN}}$ . Moreover, the inclusion of  $\kappa_{\text{NNN}}$  improves the stability of the spring network against volume collapse.

### B. Relating the CONDOR model to artificial tissue

In artificial tissue experiments, where cell-laden hydrogels are cast into molds, two key parameters control how cells interact with the ECM: (1) the cell density in the hydrogel and (2) the density of biopolymers in the hydrogel (for example collagen). In this section, we describe how parameters of the CONDOR model and artificial tissue

can be related.

Samples grown in cylindrical wells undergo larger contraction as seeding density increases, until contraction saturates at high densities. The cell-driven contraction of hydrogels cast into multiwell plates is shown in Fig. 6. Note that data for 24- and 96-well plates have been combined to get an estimate of the overall variance of the contraction associated with the growth techniques used.

To understand why contraction of artificial tissue samples saturates at large seeding densities, we consider how regions within which cells influence the ECM overlap as density increases. If density is low, the volume of influence increases linearly with cell density. However, at high density the volumes of influence around each cell start to overlap, so increasing the density further does not increase the overall volume of ECM that is influenced by the cells.

The influence of this overlap on the contraction can be estimated for a random distribution of cells, and used to arrive at a functional form to relate cell density,  $\rho$ , to  $\Delta$ . We denote the volume of influence for a single cell as  $V_{\text{infl}}$ , and the volume of influence of all  $n$  cells as  $V_{\text{tot},n}$ . Note that  $V_{\text{tot},n} < nV_{\text{infl}}$ , since the volumes of influence can overlap when cells are densely packed.

The mean additional volume of ECM, influenced by

adding the  $n$ th cell, is  $V_{\text{infl}}(1 - V_{\text{tot},n-1}/V_0)$ . This can be determined by considering the effect of adding an additional cell to a set of  $n - 1$  cells. When the  $n$ th cell is added, the probability that its volume of influence overlaps with that of existing cells is  $V_{\text{tot},n-1}/V_0$ , which is the ratio of  $V_{\text{tot},n-1}$  (the volume of influence of the existing  $n - 1$  cells) and  $V_0$  (the total volume of the tissue). Thus, the probability that the volume of influence of the new cell does not overlap is  $(1 - V_{\text{tot},n-1}/V_0)$ , and the mean additional volume of ECM influenced by the new cell can be calculated.

Thus, a recurrence relation is generated for the  $n$ th term in the expansion of the total volume of influence,  $V_{\text{tot},n}$ ,

$$V_{\text{tot},n} = V_{\text{tot},n-1} + V_{\text{infl}} \left( 1 - \frac{V_{\text{tot},n-1}}{V_0} \right) \quad (3)$$

$$= V_{\text{tot},n-1} \left( 1 - \frac{V_{\text{infl}}}{V_0} \right) + V_{\text{infl}} \quad (4)$$

$$= V_{\text{tot},n-1} R + V_{\text{infl}} \quad (5)$$

where we define,  $R = 1 - V_{\text{infl}}/V_0$ ,  $V_{\text{tot},0} = V_{\text{infl}}$ . Repeated iteration then leads to a geometric series. Since  $R < 1$  this series can be computed analytically for the volume of influence of  $N$  cells as,

$$V_{\text{infl,tot}} = V_{\text{infl}} \left( \frac{1 - R^N}{1 - R} \right). \quad (6)$$

Thus, assuming that  $\Delta \propto V_{\text{infl,tot}}$ , and since  $\rho = V_0 N = N/\rho_0$  (we define  $\rho_0 = 1/V_0$ , the density for a single cell within the tissue volume),  $\Delta \propto 1 - R^{\rho/\rho_0}$ .

Thus, the functional form relating the CONDOR model's contraction parameter,  $\Delta$ , to seeding density,  $\rho$ , is (noting that the maximum possible  $\Delta = 1$ ),

$$\Delta = 1 - R^{\rho/\rho_0}. \quad (7)$$

Without loss of generality, we define  $R' = R^{\rho_0/\rho_0}$ , so

$$\Delta = 1 - R'^{\rho/\rho'_0}. \quad (8)$$

Since  $R'$  and  $\rho'_0$  are independent, we fix  $R' = 1/2$  and allow  $\rho'_0$ , to set the density for crossover between the dilute and saturated regimes. With this choice, Eq. 8 has the correct linear form for  $\rho \ll \rho'_0$ , saturates for  $\rho \gg \rho'_0$  and has  $\Delta = 1/2$  for  $\rho = \rho'_0$ .

Eq. 8 may be inverted to determine  $\rho$  from  $\Delta$ :

$$\rho = \rho_0 \ln(1 - \Delta) / \ln(1/2). \quad (9)$$

### C. Computational method

We determine cell orientations and positions using a simulated annealing approach to find the lowest energy configuration of the cell-spring network. Bischofs and

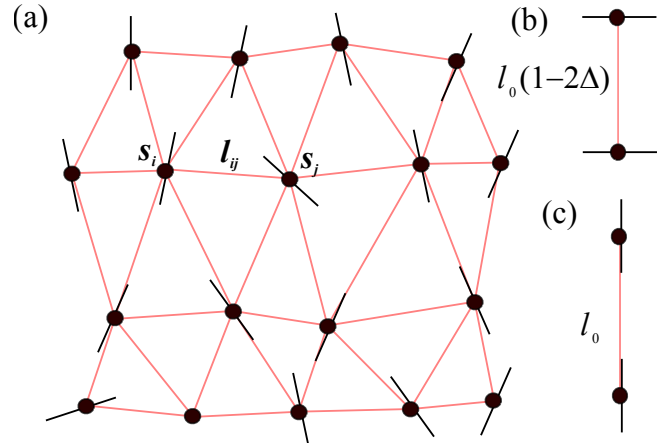


FIG. 2. (a) Schematic of the CONDOR model, showing cells at the vertices of a triangular spring network. Springs represent the extracellular matrix. Vertices are indexed as  $i$  and  $j$ . The distance between cells is  $l_{ij}$ , and cell orientation at each vertex is labeled  $\hat{s}_i$ ; (b) If cells are perpendicular to a bond, then cell generated forces reduce equilibrium length by  $2l_0\Delta$ ; (c) If cells are parallel to the bond, then equilibrium length is unchanged at  $l_0$ . 3D calculations presented here use FCC networks with next and next-next nearest (NN and NNN) neighbor spring constants  $\kappa_{\text{NNN}}/\kappa_{\text{NN}} = 0.4$ .

Schwarz have proposed that cells find an orientation consistent with the minimum work needed to obtain that configuration [11], i.e. the ground state. With a sufficiently slow anneal, the global minimum energy is guaranteed [14, 15].

In the simulated annealing approach [14, 15], a set of Monte Carlo updates are made, where in each update we modify either cell positions or orientations (or both), for either single cells or groups of cells. Cell positions and orientations are characterized using azimuthal and polar angles ( $\theta$  and  $\phi$ ) and their coordinates ( $x, y$  and  $z$ ). Updates are accepted or rejected according to a Metropolis scheme, with probability  $\exp(-\Delta E/\eta)$ , where  $\eta$  is slowly reduced according to either an exponential or fast schedule.  $\Delta E$  is the change in energy due to an update.

During reorientation, both angles are updated either from a Lorentzian distribution [15] or a stepped distribution. For the Lorentzian distribution, angles are updated according to  $\theta \rightarrow \theta' = \theta + \Delta\theta \tan(\pi(r - 1/2))$ . Here  $r$  is a random variate with range  $[0, 1]$ , computed using the `ran2` function from Press *et al.* [16]. The alternative step function update is  $\theta \rightarrow \theta' = \theta + \Delta\theta(r - 1/2)$ , where  $\Delta\theta$  characterizes range. Additional updates with  $\Delta\theta' = \Delta\theta/10$  and  $\Delta\theta'' = \Delta\theta/100$  are also used. Similar updates are made for  $\phi$ .

A major difference between this and previous work [11, 17] is that cells can move to any location, thus allowing structural changes of the tissue to be explored. Lorentzian and step updates are made for  $x, y$  and  $z$ . A fixed penalty is imposed on cells that move outside the working area of the mold. Within tethering regions, cells are not permitted to move, but can reorient.

Annealing is carried out using several anneal speeds, two anneal schedules and fixed/variable update ranges, with the lowest energy configuration from the different attempts selected for analysis. Various annealing schedules were used, including fast annealing and exponential annealing. The initial  $\eta$  was selected by increasing  $\eta$  with fixed update range until a high acceptance rate was achieved. Various schemes for selecting update range were used, including scaling of  $\Delta\theta$ , etc, with  $\eta$  so that updates are accepted with roughly equal rate throughout the anneal. For variable update range, the algorithm is considered to be finished when the ranges are less than a threshold, whereas for fixed range the algorithm finishes once the acceptance rate drops below a preselected value.

Following the anneal, the lowest energy configuration is used to calculate tensions in the springs and contraction ratios. For consistency between contractile networks with different length scales, we introduce a dimensionless tension,  $\bar{T} = \sum T/\kappa_{\text{NN}}l_0$ . This measurement describes the tension in the environment of a cell.

For the pillar arrangements, we carry out an additional analysis of experimental cell orientations from the original confocal micrograph using Volocity, for comparison with theoretical predictions (PerkinElmer, Waltham, MA, USA). Experimental details for the growth of glial cells can be found in Refs. 5, 18–20, and other experimental results have been reported elsewhere.

### III. RESULTS

#### A. Untethered tissues in wells

Computational simulations of free-floating (i.e. untethered) artificial tissue grown in cylindrical wells show increased contraction as  $\Delta$  gets bigger. Figure 3 shows top view theoretical calculations for the cell orientation in free-floating artificial glial tissue grown in 96-well plates for a variety of  $\Delta$  values. For the 96 well plates, the ratio of initial gel height to diameter is  $\sim 0.1$ . Domains are visible in the cell orientations. Shapes are similar to the experiments shown in Fig. 1(a).

From these calculations, the contraction,  $\Delta r/r_0$  vs.  $\Delta$  can be determined for free-floating gels in cylindrical wells, and is found to increase monotonically, saturating at  $\sim 50\%$  contraction. Figure 4 shows  $\Delta r/r_0$  for simulations with various  $\Delta$  values for free-floating (i.e. untethered) artificial glial tissue grown in circular 24-well and 96-well plates [21]. The ratio of initial thickness to well diameter is  $\sim 0.2$  in the 24-well plates. Contractions in the horizontal plane are shown, since they correspond to measured experimental contractions. For free-floating gels, contraction tends towards  $\sim 50\%$  as  $\Delta \rightarrow 1$ . The depth of gel does not contribute strongly to the size of the contraction, as also found experimentally [22].

A linear interpolation of Fig. 4, combined with the experimentally measured contractions, is used to determine

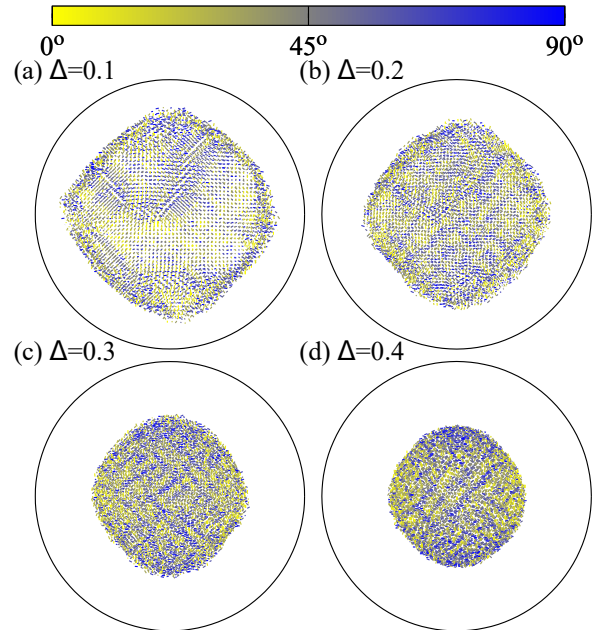


FIG. 3. Simulations show that free-floating artificial glial tissue contracts with increased  $\Delta$ , with cell orientations showing domain boundaries. Data correspond to 96-well plates. Black solid lines denote the perimeter of the well. At the start of the simulation, cells are uniformly distributed within the well. The tissue within the molds is three-dimensional, but shown in profile.

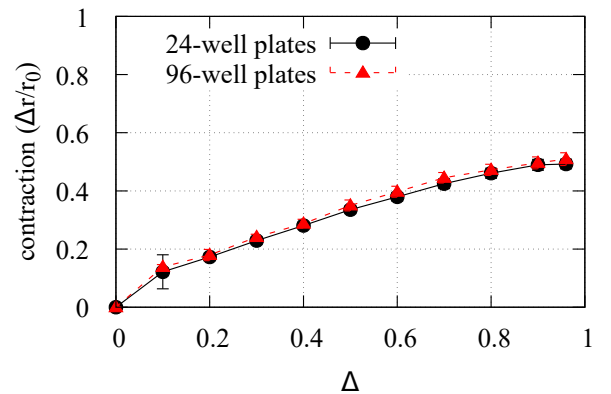


FIG. 4. Simulations predict that contraction increases with  $\Delta$  for free-floating (i.e. untethered) artificial glial tissue, with contraction saturating at around 50%. Calculations correspond to 96-well plates.

how  $\Delta$  relates to  $\rho$ . Experimental data were collected for two cell types, the C6 glioma line and primary rat astrocytes. Ranges of  $\Delta$  are determined from the experimental variance. Calculations corresponding to 96-well plates were used.

The resulting data are used to determine  $\rho_0$  using a least squares fit, showing that the functional form of Eq. 8 is consistent with the experimental data

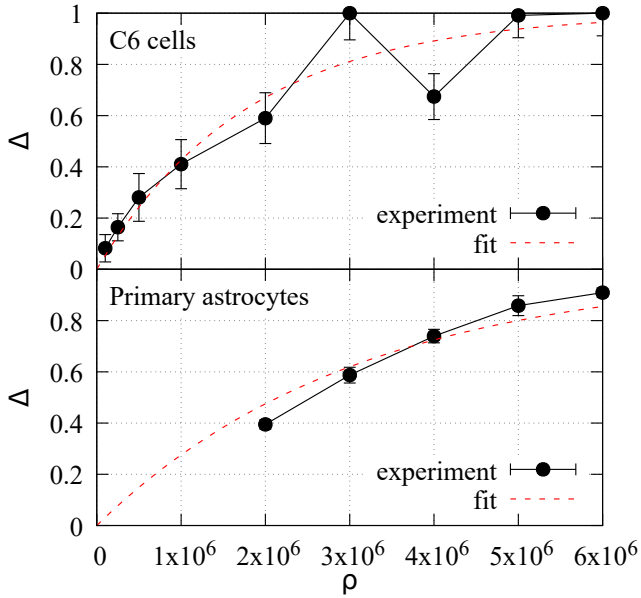


FIG. 5. A linear interpolation of Fig. 4 is used to determine how  $\Delta$  relates to  $\rho$ , with ranges of  $\Delta$  determined from the contraction in 96- and 24-well plates, and the resulting plot used to determine  $\rho_0$  using a least squares fit.

(Fig. 5). For C6 cells,  $\rho'_0 = 1.24(8) \times 10^6$  cells/ml with a lower bound on the 95% confidence interval of  $\rho'_{0,-} = 0.79(8) \times 10^6$  cells/ml and upper bound  $\rho'_{0,+} = 1.69(7) \times 10^6$  cells/ml. For primary astrocytes,  $\rho'_0 = 2.15(1) \times 10^6$  cells/ml with confidence interval  $\rho'_{0,-} = 1.67(7) \times 10^6$  cells/ml to  $\rho'_{0,+} = 2.62(4) \times 10^6$  cells/ml.

Using these values to determine the contraction for free-floating (i.e. untethered) tissue in cylindrical wells, agreement is found between the contraction vs. density curves for theory and experiment (Fig. 6). Of course, this is to be expected, since a combination of theoretical and experimental values were used to find  $\rho'_0$ , however agreement would not be possible if the the functional form in Eq. 8 were not reasonable. Both theoretical predictions and experimental measurements are shown. The area measured in experiment has been converted to an effective radius to calculate the contraction.

### B. I-shaped tethers

$\Delta$  can also be determined directly from the contraction of tissues in 96-well plates, leading to good agreement between theoretical and experimental contraction for an I-shaped system containing anti-CD49 antibodies that block integrins. Figure 7 shows a comparison of experimental results (shape) and theoretical predictions (shape and cell orientations) for artificial glial cells in an I-shaped clamp. C6 cells of density  $\rho = 4 \times 10^6$  cells/ml form the artificial tissue.

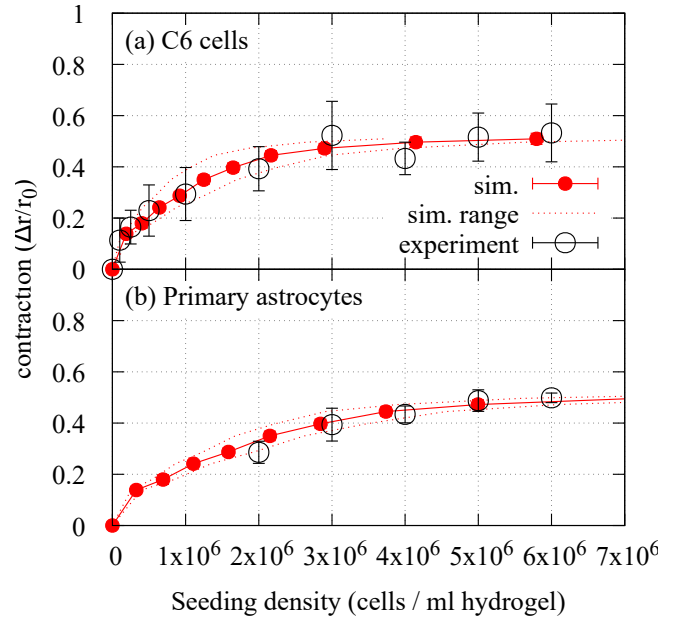


FIG. 6. Experimental contraction data match simulations of free-floating artificial tissue in wells.

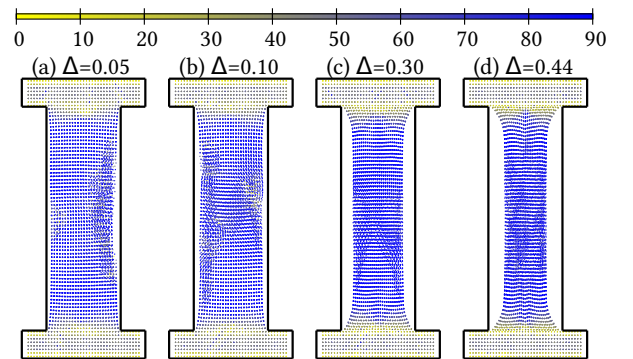


FIG. 7. Theoretical predictions for the shape of artificial glial tissues tethered in an I-shaped clamp match experimental tissues shown in Fig. 1. Cell alignments are also shown. All panels correspond to C6 cells with  $\rho = 4 \times 10^6$  cells/ml. (a)  $\Delta = 0.05$  to  $1 \mu\text{g/ml}$  anti-CD49; (b)  $\Delta = 0.1$  to  $0.3 \mu\text{g/ml}$  anti-CD49; (c)  $\Delta = 0.3$  to  $0.1 \mu\text{g/ml}$  anti-CD49; (d)  $\Delta = 0.44$ , without anti-CD49.

If 96-well data from Ref. [5] are used directly to set  $\Delta$ , agreement is good between theoretical predictions and experimental measurements of contraction for C6 cells tethered in an I-shaped clamp for hydrogels infused with various concentrations of anti-CD49 antibodies (Fig. 8). We note that contraction of the hydrogel in the I-shaped clamp is smaller than predicted if Eq. 8 is used to set  $\Delta$ . The consequences of this for calibration of the CONDOR model will be discussed later.

An important benefit of the approach presented here is the ability to gain insight into quantities that would be difficult or impossible to determine experimentally, such

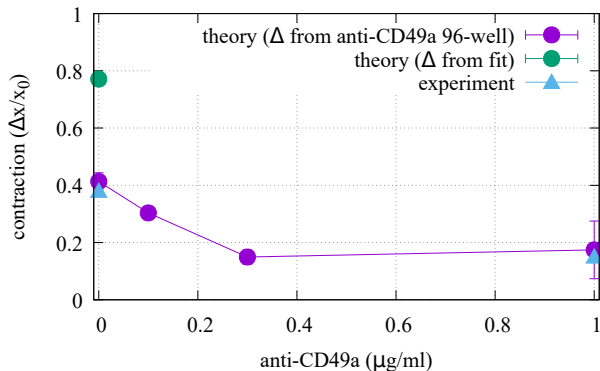


FIG. 8. If 96-well data from Ref. [5] are used directly to set  $\Delta$ , good agreement is found between theoretical predictions and experimental measurements of contraction for C6 cells tethered in an I-shaped clamp for hydrogels infused with various concentrations of anti-CD49 antibodies. Agreement is poor if Eq. 8 is used to set  $\Delta$ .

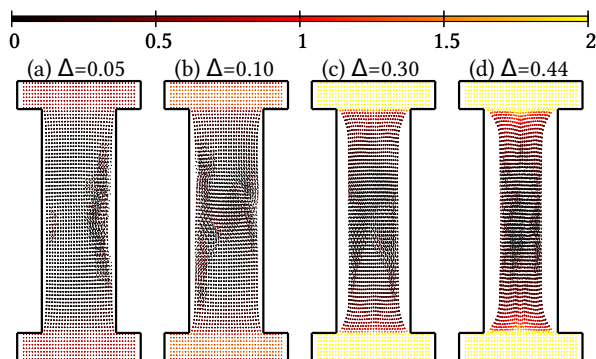


FIG. 9. Tension in simulated tissue in an I-shaped clamp show regions of high tension around the clamps. The color represents  $\bar{T}$ , with yellow representing regions of highest positive tension, red regions of moderate tension and black regions of lowest tension.

as tension. In Fig. 9, we show theoretical predictions of the tension in free-floating artificial glial tissue grown in an I-shaped mold. In well-aligned regions, tension is low. Frustration associated with rapid changes of alignment with position leads to high tension close to the clamps. This high-tension region is Delta-shaped. Insight into difficult-to-measure quantities could be used when designing bespoke clamps for artificial tissue with specific structures.

### C. Pillar tethers

In a mold where pillars are used to tether the hydrogel, interactions between cells and ECM also lead to narrowing of the artificial tissue, as seen in confocal micrograph images (Fig. 10(a)). The artificial tissue starts as an un-tensioned rectangular type I collagen gel seeded with glial cells tethered by a set of four pillars to the left and right

of the image. It obtains a bow-tie shape after 24 hours of incubation. C6 cells of density  $\rho = 4 \times 10^6$  cells/ml form the tissue.

The pillar-tethered hydrogel has a triangular (Delta) region just to the right of the two left-hand pillars, a region aligned along the short axis between the pillars and a region of glial cells aligned along the long axis towards the center of the sample (Fig. 10(b)). Volocity (PerkinElmer, Waltham, MA, USA) is used to determine cell alignments. Yellow indicates cells aligned along the short axis, and blue indicates cell alignment along the long axis. Approximately 10 000 cells are identified in the confocal micrograph image. We note that the sample has been compressed under a cover slip.

Computer simulations of cells in a pillar-like mold reproduce key features of experimental data: regions of self-organized cell alignment can be seen between the pillars and along the long axis at the center of the sample, and regions of mixed orientations are found where regions of different alignment meet (Fig. 10(c)). The positions of cells in the CONDOR model are fixed around the pillar, but permitted to change angle. All other cells are allowed to relax their positions. Results are shown for  $\Delta = 0.8$  and  $l_0 = 100\mu\text{m}$  (panel (c)). Calculations contain 59 891 cells.

Regions of highest dimensionless tension,  $\bar{T}$  are associated with regions of rapidly changing cell orientation, as in the tissues simulated in I-shaped molds. The strongest tension can be found in the small region between the pillars, extending into a roughly triangular shape of higher tension along the long axis (Fig. 10(d)). So again, higher tension is associated with regions of rapidly changing alignment. The color represents the dimensionless value  $\bar{T}$ , with yellow representing regions of highest positive tension, red regions of moderate tension and black regions of lowest tension.

Contraction at the center of the sample is consistent between experiment and theory (Fig. 11). The value of contraction using  $\Delta$  extracted from  $\rho'_0$  is slightly higher than the experimental value, however the experimental contraction is close to the contraction determined using the lower confidence interval of  $\rho'_0$  (shown using dashed lines).

## IV. DISCUSSION AND CONCLUSIONS

In this paper, we have introduced the CONDOR model, a biophysical model that combines contractile network and force-dipole models, to describe the feedback between cells and the extracellular matrix in artificial glial tissue. In the CONDOR model, a network of springs represents ECM and the active forces generated by cells are represented by an additional contraction with a dipole symmetry. The lowest energy configuration of the CONDOR model is found using simulated annealing. Results from the CONDOR model match experimental results of artificial tissue, both on a microscopic level

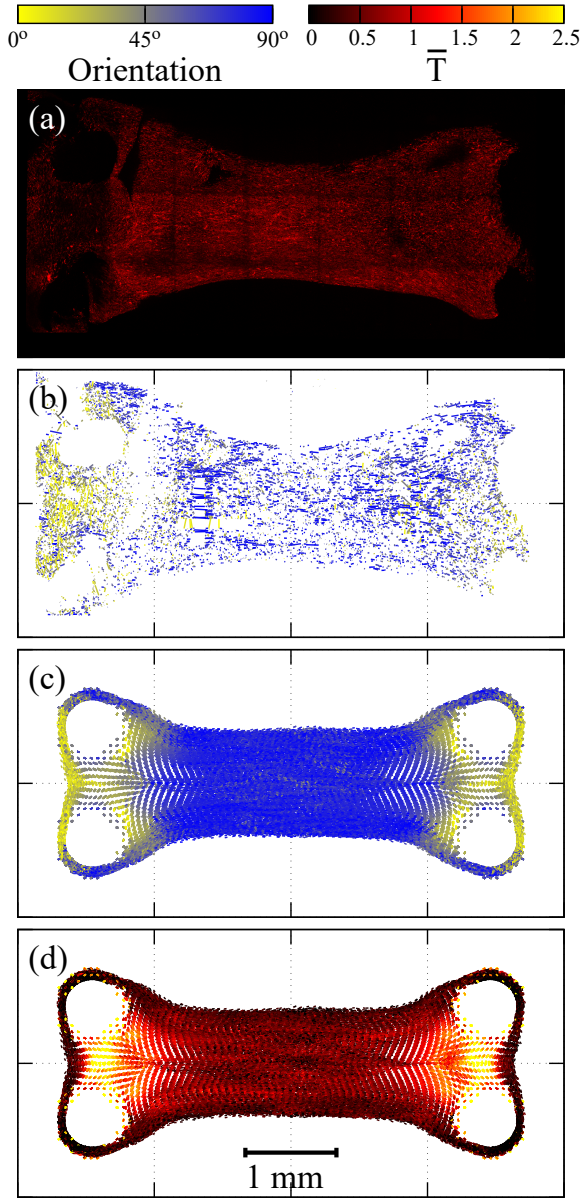


FIG. 10. Good agreement is found between both shape and cell orientation in experimental data and simulations for artificial tissue tethered with vertical pillars. (a) A confocal micrograph of the engineered tissue was taken, with tethering holes visible on the left of the image and a characteristic bow-tie shape; (b) Cell orientations extracted from the micrograph; (c) Theoretical results show self-organized cell alignment along the long axis and also along the short axis between tethers, with a region of various orientations at the interface between the two, as in the experimental data; (d) Moderate tension is found in the central region, which is aligned along the long axis. Regions of low tension are seen at the edge of the sample. Mixed tensions are found in the triangular region of mixed orientations. Regions of highest tension correspond to the region aligned along the short axis between the pillars.

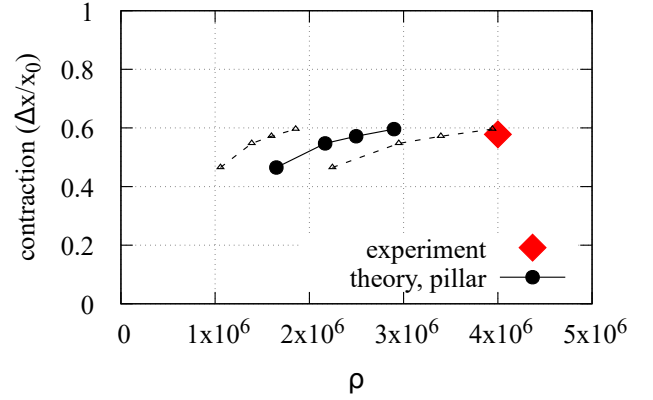


FIG. 11. Comparison between experimental and theoretical predictions of contraction for artificial tissue grown within pillar molds. Dashed lines with small triangles represent standard error range of  $\rho$  values obtained from  $\Delta$ .

from cell alignments, and on a macroscopic level for the shapes of tethered tissues.

We develop a biophysical model for predicting self-organization and reshaping of artificial tissue due to the microscopic active forces between cells and the extracellular matrix (ECM), which we solve using simulated annealing, obtaining close agreement with experiment.

To our knowledge, this is the first biophysical model that combines contractile networks and force dipoles, to predict self-organization and reshaping of tissue due to the microscopic active forces between cells and the ECM. Force dipoles have been a popular approach for describing the interactions between cells and the ECM [10]. For example, the interactions of dipolar and multipolar cells with external strain fields and with each other have been investigated [11, 23–26]; further studies of many-body effects between small numbers of cells with fixed positions have been carried out using Monte Carlo simulations [17]; applications to the self-polarization of cells in elongated gels have been investigated [27]; and the onset of order in muscle tissue has been studied [28]. The force-dipole approach has provided insight into the reasons that cells orient, especially in response to external stresses. While force-dipole models are undoubtedly sophisticated, repulsive terms leading to finite compressibility of the viscoelastic ECM are not present. To stop collapse, cells in these theoretical models are constrained either to fixed positions, or small movements about such fixed positions. Cells in tissues are not constrained in this way. Thus pure force-dipole models do not incorporate the feedback between self-organization and reshaping driven by active forces that are found in real tissues. On the other hand, contractile network models have been used to describe the shapes of both tethered single cells and bulk tissues, but not the active forces between cells and ECM [6–8].

The CONDOR model has several key strengths, including:

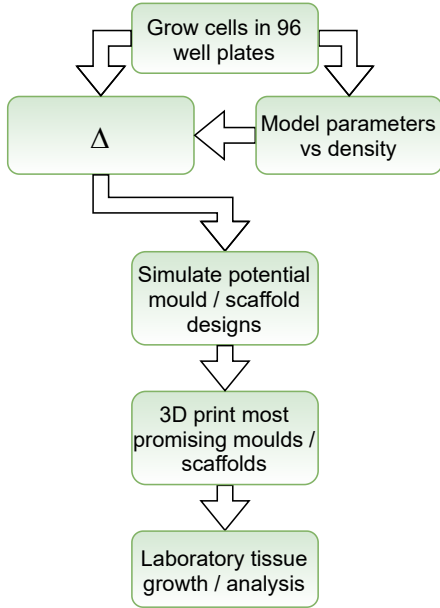


FIG. 12. Procedures for predictive simulation of self-organization in artificial tissue samples.

1. Accurate description of the self-organization and reshaping of tissue that is driven by the feedback between cells and ECM.
2. Predictive capability for the shapes of tissues and the orientations of cells in those tissues.
3. Simplicity (with similarities to the Heisenberg model of spin alignments), allowing for simulation of large numbers of cells ( $\gtrsim 10^5$ ).
4. Generalizability to different symmetry arrangements by adding higher order multipolar corrections or other alternative symmetries to  $f(\theta)$ .
5. Extensibility to disorder, which can be achieved by including random bonds or by making corrections to the equilibrium distances of bonds.

Specific patterns of cellular self-organization are important in many tissues, making it challenging to grow artificial tissues that properly represent those in living organisms. The use of artificial or engineered tissue for regenerative medicine has the potential to significantly improve human health [29] and provide new biological models for drug testing [30]. The cells in real tissues are typically arranged in ways that may be difficult to reproduce artificially. This is a particular problem for nerve tissue, which must be well-ordered to function properly. In the nervous system, neurons are typically

guided by glial cells, so well-ordered glial cells in artificial tissue could lead to well-directed neuron growth for, e.g., nerve repair. For nerve regeneration applications, favorable characteristics are high levels of cell alignment and cross-section that is uniform along the length of the tissue, while regions of misalignment around tethering points should be minimized.

Design of artificial tissue with realistic characteristics is something that is very difficult and time consuming to do using trial and error. Particularly relevant experimental parameters include cell density and distribution (e.g. the results of uneven distributions or gradients of cells) and ECM density and stiffness. These parameters are expensive and time-consuming to investigate experimentally, so the ability to run simulations to predict outcomes would be extremely valuable.

Simulations using the CONDOR model described here are fast enough to assist the rational design of experimental molds and scaffolds that guide artificial tissue growth. A procedure is proposed in Fig. 12. The experiments that we compare to in this paper were carried out with the usual care to control confounding variables such as passage (which is integer and can be matched exactly) and confluency, which is controlled to around 60-70% [31]. However, even with this care, there can be large variations in tissue contraction, due, not only to these variables, but also since the tissue can sometimes adhere to the sides of the mold in addition to the tethering points. This variation leads to sizable uncertainties in the value of  $\rho'_0$  for a particular cell type. Determination of  $\Delta$  from multi well plates is particularly sensitive to statistical fluctuations in experimental results due to the slow change in contraction with  $\rho$ , especially at larger  $\rho$  values. We note that where tethered molds and 96-well plates are seeded with precisely the same cell batch, as discussed with I-shaped molds, the agreement between theory and experiment is very close. The comparison with experiment carried out here indicates that for a design process, a broad range of  $\Delta$  should be used to obtain indicative results for specific mold designs.

Future work will extend the CONDOR model to improve predictions of self-organization in tissue, with increased sophistication to improve the description of the ECM, the cell response to tension in the ECM, and time-dependence: (1) By describing tissues as active continuum materials [32], the CONDOR model could be extended for tightly-packed cells (since cells would be able to interact directly in that scenario). (2) Extension to agent-based simulations to introduce time dependence, to study, e.g. the evolution of samples during their growth phase [5], or oscillatory strain stimuli (e.g. [33–35]). (3) By modifying the CONDOR model to allow cells to be unpolarized in regions of low tension. The cells in the CONDOR model are always elongated (polarized), however experimental systems have regions where cells are not elongated, particularly within the Delta region, so the contraction of the sample may be over-estimated. (4) To include randomized spring networks to better describe

collagen networks in the ECM. Work to carry out these extensions is currently in progress.

Another intriguing possibility for further work is the investigation of phase transitions between self-organization and disorder in the CONDOR model. Within the tissue bulk, cells order along a single direction. Disorder introduced through the breaking of translational symmetry in the spring network via random connections between cells has potential to frustrate this order. Overall, we expect that a wide range of interesting

biophysics can be studied within extensions to the CONDOR model introduced here.

## ACKNOWLEDGMENTS

The authors would like to thank Dr. Calum McCormick for useful discussions. The authors have no competing interests.

- 
- [1] M. Georgiou, S. C. Bunting, H. A. Davies, A. J. Loughlin, J. P. Golding, and J. B. Phillips. *Biomaterials*, 34:7335–43, 2013.
- [2] J. B. Phillips, S. C. Bunting, S. M. Hall, and R. A. Brown. *Tissue Eng.*, 11:1611–7, 2005.
- [3] D. Mukhey, J.B. Phillips, J.T. Daniels, and A.K. Kureshi. *Acta Biomaterialia*, 67:229, 2018.
- [4] E. East, D. B. De Oliveira, J. P. Golding, and J. B. Phillips. *Tissue Eng. Part A*, 16:3173–84, 2010.
- [5] C. O’Rourke. PhD thesis, Open University, 2016.
- [6] P. Guthardt Torres, I. Bischofs, and U. Schwarz. *Phys. Rev. E*, 85:011913, 2012.
- [7] I. B. Bischofs, F. Klein, D. Lehnert, M. Bastmeyer, and U. S. Schwarz. *Biophysical Journal*, 95(7):3488 – 3496, 2008.
- [8] I. B. Bischofs, S. S. Schmidt, and U. S. Schwarz. *Phys. Rev. Lett.*, 103:048101, 2009.
- [9] M. Eastwood, V.C. Muder, D.A. McGrouther, and R.A. Brown. *Cell Motil. Cytoskeleton*, 40:1321, 1998.
- [10] U. S. Schwarz and S. A. Safran. *Rev. Mod. Phys.*, 85:1327–1381, 2013.
- [11] I. B. Bischofs and U. S. Schwarz. *Proc. Natl. Acad. Sci. USA*, 100:9274–9279, 2003.
- [12] D. H. Boal. Cambridge University Press, Cambridge, UK, 2nd edition, 2012.
- [13] P. Kollmannsberger, C. M. Bidan, J. W. C. Dunlop, and P. Fratzl. *Soft Matter*, 7:9549–9560, 2011.
- [14] S. Kirkpatrick, C. D. Gelatt, M. P. Vecchi, et al. *Science*, 220:671–680, 1983.
- [15] H. Szu and R. Hartley. *Physics Letters A*, 122:157–162, 1987.
- [16] W. Press, S. Teukolsky, W. Vetterling, and B. Flannery. Cambridge University Press, Cambridge, UK, 1992.
- [17] I. B. Bischofs and U. S. Schwarz. *Acta Biomaterialia*, 2:253–265, 2006.
- [18] C. O’Rourke, R. A. Drake, G. W. Cameron, J. A. Loughlin, and J. B. Phillips. *Journal of Biomaterial Applications*, 30:599–607, 2015.
- [19] K. Sanen, R. Paesen, S. Luyck, J.B. Phillips, I. Lambrechts, W. Martens, and M. Ameloot. *Acta Biomaterialia*, 30:258–64, 2016.
- [20] J. B. Phillips and R. A. Brown. volume 695 of *Methods in Molecular Biology*, pages 183–196. Humana Press, 2011.
- [21] For those not familiar with cell culture terminology these are standardized trays with circular depressions for growing and analyzing cells and tissues, with the number referring to the number of depressions within the tray.
- [22] Additional data showing change in contraction with depth, and for 24 well plates, provided by C. O’Rourke can be found in the supplementary material.
- [23] I. B. Bischofs, S. A. Safran, and U. S. Schwarz. *Phys. Rev. E*, 69:021911, 2004.
- [24] I. B. Bischofs and U. S. Schwarz. *Phys. Rev. Lett.*, 95:068102, 2005.
- [25] A. Zemel, I. B. Bischofs, and S. A. Safran. *Phys. Rev. Lett.*, 97:128103, 2006.
- [26] U. S. Schwarz and S. A. Safran. *Phys. Rev. Lett.*, 88:048102, 2002.
- [27] A. Zemel and S. A. Safran. *Phys. Rev. E*, 76:021905, 2007.
- [28] B. M. Friedrich, A. Buxboim, D. E. Discher, and S. A. Safran. *Biophysical Journal*, 100:2706, 2011.
- [29] F.J. O’Brien. *Materials Today*, 14(3):88 – 95, 2011.
- [30] C. O’Rourke, C. Lee-Reeves, R. A. L. Drake, G. W. W. Cameron, A. J. Loughlin, and J. B. Phillips. *Journal of Tissue Engineering*, 8:1–9, 2017.
- [31] For those not familiar with cell culture terminology, confluency refers to the cell density in the flask used to grow cells. At a low confluency the cells can multiply freely. At high confluency, crowding of cells slows their multiplication rate. Confluency also affects contraction. Ideally cells should be used at 60-70% confluence. Eventually, cells need to be detached from the flask and either used for experiments or divided between a number of flasks to expand and increase in number. Each time cells are divided between flasks, passage number is incremented. For many cell types, growth rate decreases with increased passage number and again contraction can also be affected.
- [32] A. Doostmohammadi, J. Iñes-Mullol, J. M. Yeomans, and F. Sagus. *Nature Communications*, 9:3246, 2018.
- [33] R. De, A. Zemel, and S. A. Safran. *Nature Physics*, 3:655–659, 2007.
- [34] R. De and S.A. Safran. *Phys. Rev. E*, 78:031923, 2008.
- [35] S. A. Safran and R. De. *Phys. Rev. E*, 80:060901, 2009.